Phys Chem Minerals (2004) 31: 142–154
DOI 10.1007/s00269-003-0370-y

ORIGINAL PAPER

B. A. Kolesov · C. A. Geiger

A Raman spectroscopic study of Fe–Mg olivines

Received: 6 February 2003 / Accepted: 16 October 2003

Abstract End-member synthetic fayalite and forsterite and a natural solid-solution crystal of composition $(Mg_{1.80},Fe_{0.20})SiO_4$ were investigated using Raman spectroscopy. Polarized single-crystal spectra were measured as a function of temperature. In addition, polycrystalline forsterite and fayalite, isotopically enriched in ^{26}Mg and ^{57}Fe, respectively, were synthesized and their powder spectra measured. The high-wavenumber modes in olivine consist of internal SiO_4 vibrations that show little variation upon isotopic substitution. This confirms conclusions from previous spectroscopic studies that showed that the internal SiO_4 vibrations have minimal coupling with the lower-wavenumber lattice modes. The lowest wavenumber modes in both forsterite and fayalite shift in energy following isotopic substitution, but with energies less than that which would be associated with pure Mg and Fe translations. The low-wavenumber Raman modes in olivine are best described as lattice modes consisting to a large degree of mixed vibrations of M(2) cation translations and external vibrations of the SiO_4 tetrahedra. The single-crystal spectra of forsterite and $Fo_{90}Fa_{10}$ were recorded at a number of temperatures from room temperature to about 1200 °C. From these data the microscopic Grüneisen parameters for three different A_g modes for both compositions were calculated, and also the structural state of the solid solution crystal was investigated. Small discontinuities observed in the wavenumber behavior of a low-energy mixed Mg/T(SiO_4) mode between 700 and 1000 °C may be related to minor variations in the Fe–Mg intracrystalline partitioning state in the $Fo_{90}Fa_{10}$ crystal, but further spectroscopic work is needed to clarify and quantify this issue. The mode wavenumber and intensity behavior of internal SiO_4 vibrations as a function of temperature are discussed in terms of crystal field and dynamic splitting and also v_1 and v_3 coupling. Crystal-field splitting increases only very slightly with temperature, whereas dynamical-field splitting is temperature dependent. The degree of v_1–v_3 coupling decreases with increasing temperature.

Keywords Olivine · Forsterite · Fayalite · Raman spectroscopy · Isotopic substitution · High-temperature measurements · Cation order–disorder

B. A. Kolesov
Institute of Inorganic Chemistry,
Lavrentiev prosp. 3,
Novosibirsk 630090, Russia

C. A. Geiger (✉)
Institut für Geowissenschaften,
der Universität Kiel, Olshausenstr. 40,
24098 Kiel, Germany
e-mail: chg@min.uni-kiel.de
Fax: 0431-880-4457
Tel: 0431-880-2895

Introduction

Olivine is an important rock-forming silicate and is the most abundant phase of Earth's upper mantle. It has been the subject of much structural, crystal chemical, and thermodynamic study because of its petrological and geophysical significance. It has the general formula [M(1)M(2)SiO_4], where M = Fe^{2+}, Mg, and Mn^{2+} for most natural crystals. Most rock-forming olivines are binary Fe–Mg solid solutions consisting of the isostructural end members forsterite (Fo), Mg_2SiO_4, and fayalite (Fa), Fe_2SiO_4. Olivines of the upper mantle are Mg-rich with a composition of approximately $Fo_{88}Fa_{12}$, but a complete exchange of Fe^{2+} and Mg over the two crystallographically independent octahedral M sites is possible and fayalite-rich crystals are found in certain geologic environments. Compared to other rock-forming silicates, there has been a good deal of vibrational spectroscopic and lattice dynamic study made on olivine, because its small unit cell and relatively simple orthosilicate structure afford detailed analysis (Fig. 1). Atomistic-scale and lattice-dynamic study, when combined with the solid base of structural, crystal-chemical, and thermodynamic data that exists for olivine, enables

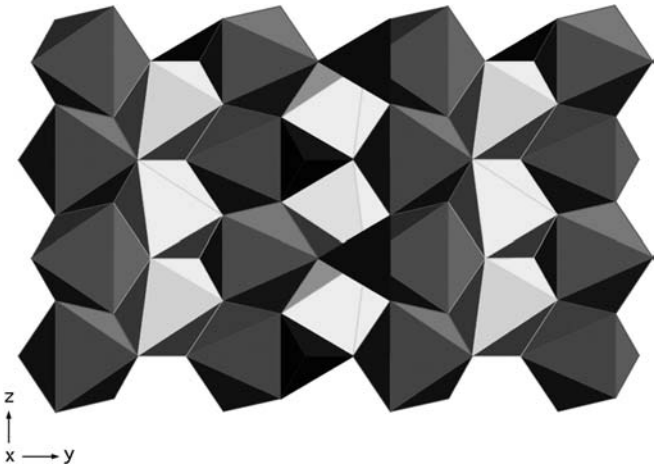

Fig. 1 Polyhedral model of the forsterite structure projected onto (100) in space group *Pbnm*. The *light-shaded* octahedra are the M(1) sites and the *darker-shaded* ones M(2). The SiO_4 tetrahedra are *dark colored*

prediction of olivine's behavior under different pressure and temperature conditions. It also provides valuable insight that can be used to interpret or understand the macroscopic thermodynamic functions like heat capacity and bulk physical properties such as thermal expansion and compressibility.

A number of IR and Raman spectroscopic investigations have been carried out over the years on both synthetic and natural olivines. The quality of the spectra has improved continuously and the more recent measurements have extended the investigations into the high-temperature and high-pressure regimes. In addition, inelastic neutron scattering studies (Rao et al. 1988; Ghose et al. 1991; Price et al. 1992; Schmidt et al. 1992) have been very useful in interpreting the lattice-dynamic properties of forsterite and fayalite. Pâques–Ledent and Tarte (1973) made some of the first powder IR and Raman measurements on synthetic end-member forsterite using ^{28}Si–^{30}Si and ^{24}Mg–^{26}Mg isotopic substitution in order to assign the observed bands. However, they did not present their Raman spectra. Hohler and Funk (1973) undertook polarized single-crystal Raman and IR measurements on three different nearly end-member composition olivine-structure phases, which were forsterite-rich ($Fo_{95}Fa_5$), tephroite (Mn_2SiO_4)-rich, and monticellite ($CaMgSiO_4$)-rich, and analyzed their lattice-dynamic properties. They observed, for example, strong mode mixing at low wavenumbers, and they considered the nature of crystal-field and dynamical splitting of the internal SiO_4 vibrations. Servoin and Piriou (1973) and Iishi (1978) also presented polarized single-crystal Raman spectra of forsterite at room temperature. Piriou and McMillan (1983) made Raman measurements on different polycrystalline olivines and related phases. They concentrated their analysis on the high-wavenumber region and discussed the nature of mode coupling between internal SiO_4 vibrations. Stidham et al. (1976) measured the single-crystal Raman and IR spectra of synthetic end-member tephroite at 300 and 14 K and confirmed earlier proposals that internal SiO_4 modes do not interact greatly with the low-energy M-site cation vibrations. Chopelas (1991) undertook a single-crystal Raman study of natural and synthetic olivines, including forsterite, fayalite, and monticellite, emphasizing the low-wavenumber modes below 450 cm^{-1}, and she presented new vibrational mode assignments. The most recent single-crystal IR absorption and reflection measurements on forsterite and fayalite were made by Hofmeister (1987, 1997). She also made mode assignments by employing samples of different oxygen isotopic composition. Chopelas (1990) carried out some of the earliest Raman measurements at high pressures in a diamond anvil cell to about 20 GPa on forsterite in order to investigate its thermodynamic properties. Liu and Mernagh (1993) recorded high-pressure Raman spectra to 17 GPa on fayalite and 30 GPa on forsterite. Gillet et al. (1991) undertook a high-temperature Raman study on forsterite to about 1150 K and 10 GPa, and Gillet et al. (1997) made further high-temperature measurements on forsterite up to 2000 K in order to investigate the intrinsic anharmonicity of the Raman-active modes.

Goals of this study

In spite of these numerous studies, which have shed much light on the structural, crystal chemical, lattice dynamic, and thermodynamic properties of the olivine group of minerals, uncertainties and gaps in knowledge still persist. The following areas need more vibrational spectroscopic investigation. (1) The Raman mode assignments require further analysis, especially those in the low-wavenumber region, where many modes are best described as mixed or coupled lattice vibrations. Some of the more recent assignments (e.g., Chopelas 1991; Hofmeister 1997) differ from those of earlier studies such as those of Rao et al. (1988) that are based on inelastic neutron-scattering measurements and lattice-dynamic calculations. The best experimental method for making mode assignments in vibrational spectra, and also for investigating the nature of mode coupling and mixing, is through isotope substitution (Tarte and Preudhomme 1970). However, relatively little work, except for the early study of Pâques–Ledent and Tarte (1973), has been done using this technique for analyzing the Raman spectra of olivine. (2) A second issue of interest concerns the intracrystalline partitioning and order/disorder behavior of the M-site cations in forsterite–fayalite [$(Mg,Fe)_2SiO_4$] solid solutions. Recent in-situ neutron diffraction investigations (Artioli et al. 1995; Redfern et al. 2000; Rinaldi et al. 2000) made over a range of temperatures have shown, in contrast to the "normal" cation order/disorder behavior observed in most silicates, that ordering in olivine is greater at elevated than at lower temperatures (i.e., room temperature). Moreover, there may be a

reversal of the Mg/Fe partitioning behavior between M(1) and M(2) with increasing temperature. An important point here is that the cation-ordering state cannot be quenched in and measured at room temperature. There are no vibrational spectroscopic measurements on Fe–Mg olivine solid solution crystals that have been undertaken in-situ at high temperatures to address this issue. (3) Lastly, the role of mode splitting and coupling needs further study, as does the role of intra- and intertetrahedral force constants that affect internal SiO_4 vibrations. The latter were discussed in detail most recently by Piriou and McMillan (1983), whose analysis was largely based on measurements of different composition olivines and related structures. The nature of coupling can also be addressed by studying the effect of temperature on the olivine structure, but this has not yet been done.

In order to address these different issues, we measured the Raman spectra of synthetic end-member forsterite (^{26}Mg-enriched and of normal composition), fayalite (^{57}Fe-enriched and normal composition), and a natural Mg–Fe olivine of composition $Fo_{90}Fa_{10}$ to better understand the lattice-dynamic behavior and crystal chemistry of Fe–Mg olivines. Both powder and polarized single-crystal spectra have been recorded and at temperatures between 20 and 1200 °C.

Experimental

Olivine synthesis and characterization

Single crystals of synthetic end-member forsterite and fayalite were provided by Prof. H. Rager (Marburg) and Dr. F. Wallrafen (Bonn), respectively. The colorless forsterite crystal, containing a very small amount of Cr_2O_3, was grown by the Czochralski method and is that described in Bershov et al. (1983). The fayalite crystal used for measurement is a euhedral, doubly terminated crystal about 3 mm long and 2 mm across. It is brown in color and was grown in a $FeCl_2$ flux under an Ar atmosphere. It contains very small amounts of fine Fe particles.

Isotopically enriched polycrystalline forsterite was synthesized from an oxide mix of SiO_2 (99.99%) and enriched MgO (from the State Scientific Center of the Russian Federation, Obninsk, containing 97.10 ± 0.20% of the isotope ^{26}Mg, 1.82% ^{24}Mg and 1.08% ^{25}Mg). The two oxide powders were mixed in the proper proportions and homogenized in an agate mortar and then pressed to a pellet. The pellet was heated slowly up to 1400 °C in a chamber oven and held there for about 24 h. It was removed, finely ground, repressed to a pellet, and resintered at 1400 °C for an additional 24 h. An X-ray powder pattern of the final product showed only the presence of forsterite peaks.

Isotopically enriched fayalite was prepared by mixing together powdered SiO_2 and $^{57}Fe_2O_3$ (obtained from G. Novikov, Chernogolovka, Russia; stated purity about 90%) in proportions to yield stochiometric fayalite after the Fe_2O_3 was reduced to 'FeO'. The oxide mix was intimately mixed, ground in an agate mortar, and pressed to a pellet. The pellet was sintered at 1000 °C in a gas mixing furnace at $\log f_{O_2} = -13.5$ for about 4 days. The oxygen fugacity was controlled by using a predetermined flow of CO/CO_2. The fine-grained polycrystalline product was characterized by powder X-ray diffraction that showed only peaks belonging to fayalite. The natural olivine crystal of composition nearly $Fo_{90}Fa_{10}$ is a gemmy green-colored single crystal of approximately $2 \times 3 \times 2$ mm size and is from Zagbargad Island in the Red Sea. A microprobe analysis showed a compositionally homogeneous crystal, whose average composition, based on 21 random point analyses, is $(Mg_{1.80}Fe_{0.19})Si_{1.00}O_{4.00}$.

Raman spectroscopy

Polarized single-crystal Raman spectra were recorded with a Triplemate, SPEX spectrometer with a multichannel CCD detector, LN-1340PB, from Princeton Instruments. The 488- and 514-nm lines of an Ar laser were used for spectral excitation. The spectra of fayalite were recorded using the 632.8-nm line of a He–Ne laser, with 50 mW power, to limit melting or oxidation. All the spectra collected at room temperature were measured in backscattering geometry. In this case, the laser beam was focused to a diameter of 2 μm using an LD-EPIPLAN, 40/0.60 Pol., Zeiss objective with a numerical aperture of 0.6. The spectral resolution was 5 cm^{-1} for measurements at room temperature and above. The powder Raman spectra of forsterite and fayalite of normal and isotopically enriched composition were measured only at room temperature. Because the $^{26}Mg_2SiO_4$ and $^{57}Fe_2SiO_4$ samples are polycrystalline pellets, we compare their spectra to powder spectra obtained on normal forsterite and fayalite composition and not the single-crystal results. Powders were obtained by grinding small pieces of the single crystals. The wavenumber shifts of the bands are small and, therefore, in order to determine them precisely, we measured the spectra of the normal and isotopically enriched samples three times, and each time a new calibration of the spectrometer was made. The spectra were averaged to obtain the final wavenumbers of the different modes. The measured shifts are experimentally significant, because the positions of low-wavenumber rotational modes of atmospheric N_2 and O_2 were used as a check of our experimental precision.

The polarized single-crystal spectra in the temperature range of 20–1200 °C were made with a self-designed and self-built heating stage. The stage is small and can be placed under a microscope. The heating element consists of a graphite strip of dimensions $2.0 \times 0.7 \times 40.0$ mm. It operates to high temperatures and is not strongly deformed with heating, nor does it require a high power supply, and its construction permits one to arrange the sample in the required crystallographic orientation. Temperature was measured with a Pt–Pt(Rh) thermocouple fixed between two thin BN plates that are held against the heater from below by a spring support. The thermocouple was calibrated against the melting point of several compounds. The heating stage is enclosed inside a water-cooled brass container through which He is passed to prohibit oxidation of the graphite and the sample. A LM PlanF1, 50x/0.50, Olympus objective with a working distance of 9.6 mm, together with the 488 nm line of an Ar laser having 400–800 mW of output power, were used for the measurements.

The polarized single-crystal spectra of fayalite were recorded at roughly 100 °C temperature intervals from room temperature to about 500 °C. Temperatures are estimated to be precise to within ±10 °C. The forsterite and $Fo_{90}Fa_{10}$ samples were studied with greater care and with a larger number of measurements in order to characterize possible spectral changes resulting from changes in Fe–Mg order/disorder and partitioning behavior in the solid solution. For these measurements, the temperature was held constant for about 7 min prior to collecting a spectrum. The measurement itself took about 4 min. Measurements were made up to 1200 °C and the temperature uncertainty is estimated to be ±5 °C.

Symmetry analysis of the normal modes

Olivine is orthorhombic, space group $Pnma = D_{2h}^{16}(62)$ and it has four formula units per unit cell. The M(2), Si, O(1) and O(2) atoms are located on mirror planes and have C_s point symmetry. The M(1) cation is located at the origin of the unit cell and has C_i point

Table 1 Symmetry analysis of the normal modes for olivine of space group *Pbnm*. *T* translations; *R* hindered rotations (i.e., librations)

	M(1)	M(2)	T(SiO_4)	R(SiO_4)	$(SiO)_{bend}$		$(SiO)_{str}$	
					ν_2 (E)	ν_4 (F_2)	ν_1 (A_1)	ν_3 (F_2)
A_g	_	2, *xy*	2, *xy*	1, *z*	1	2	1	2
B_{1g}	_	2, *xy*	2, *xy*	1, *z*	1	2	1	2
B_{2g}	_	1, *z*	1, *z*	2, *xy*	1	1	_	1
B_{3g}	_	1, *z*	1, *z*	2, *xy*	1	1	_	1
A_u	3, *xyz*	1, *z*	1, *z*	2, *xy*	1	1	_	1
B_{1u}	3, *xyz*	1, *z*	1, *z*	2, *xy*	1	1	_	1
B_{2u}	3, *xyz*	2, *xy*	2, *xy*	1, *z*	1	2	1	2
B_{3u}	3, *xyz*	2, *xy*	2, *xy*	1, *z*	1	2	1	2

symmetry, while O(3) and O(4) occupy general positions of C_1 symmetry. From this, a symmetry analysis of the normal modes can be made (e.g., Hohler and Funk 1973; Stidham et al. 1976; Chopelas 1991). In the literature one can find crystallographic settings that are different from the standard one (i.e., *Pnma*). Any setting may be used for a symmetry analysis, but it will result in B_{iu} modes different from than that given by the standard setting. In the *Pbnm* setting, which is generally used in the crystallographic literature for the olivine structure (e.g., Brown 1980), the normal mode analysis as given in Table 1 is obtained. All the gerade modes are Raman-active, the ungerade modes B_{1u}, B_{2u} and B_{3u} are IR-active and the A_u modes are spectroscopically inactive. Three modes of B_{1u}, B_{2u}, and B_{3u} symmetry each are acoustic vibrations.

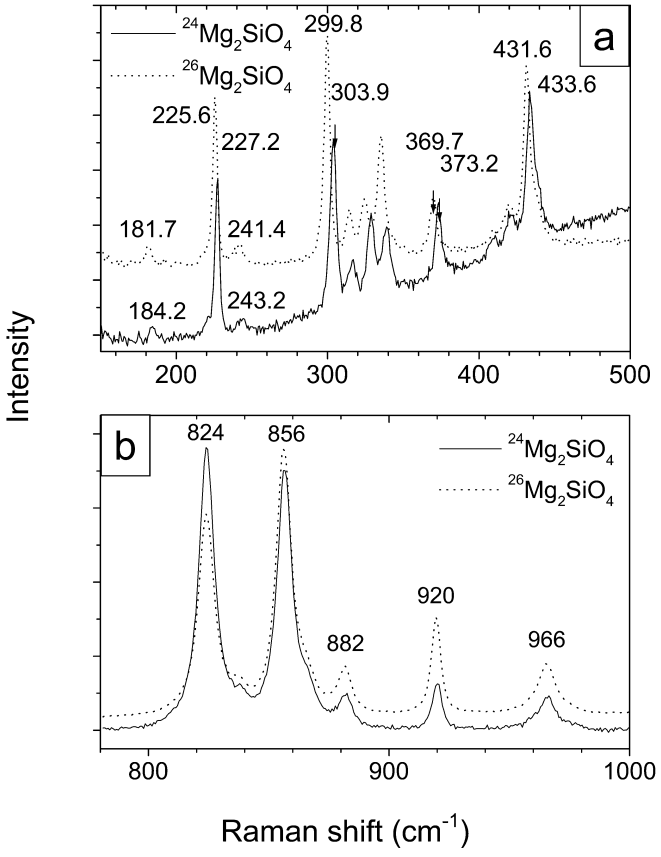

Fig. 2a, b Raman powder spectra of normal and isotopically enriched forsterite in the **a** low- and **b** high-wavenumber region

Results

Figure 2 shows the unpolarized spectra of polycrystalline, normal and ^{26}Mg-enriched forsterite in the low and high wavenumber regions. For both samples curve fitting was undertaken using Lorenztian components to determine the wavenumbers of the individual bands. In addition, some bands, which are observed in the polarized single-crystal spectrum, are not observed in the spectrum of polycrystalline forsterite. These are the B_{1g} bands at 218, 274, 351, 383, 632, and 975 cm^{-1}, those of B_{2g} symmetry at 175, 323, 363 cm^{-1}, and B_{3g} symmetry at 286 and 323 cm^{-1}. Table 2 lists the experimentally measured wavenumbers and wavenumber shifts for the different modes resulting from isotopic substitution in forsterite.

The low-wavenumber region for normal and ^{57}Fe-enriched fayalite is shown in Fig. 3. Two bands, B_{1g} at $\sim$155 cm^{-1} and A_g at $\sim$172 cm^{-1}, exhibit a relatively large isotopic shift of 1.0 and 0.8 cm^{-1}, respectively. They are depicted further in the insert in Fig. 3. A third band that displays an appreciable isotopic shift is the B_{3g} mode at $\sim$281 cm^{-1}. The high-wavenumber region of fayalite shows broad bands consisting of SiO_4-stretching vibrations that are coupled with low-energy magnetic excitations (Kolesov and Geiger, accompanying paper) and they do not exhibit large isotopic shifts. The wavenumber and isotopic shifts of the bands observed in the region of 150–530 cm^{-1} in normal fayalite and $^{57}Fe_2SiO_4$ are listed in Table 3.

The single-crystal polarized (*cc*) spectra for forsterite and $Fo_{90}Fa_{10}$ as a function of temperature are shown in Figs. 4 and 5. The spectrum of $Fo_{90}Fa_{10}$ is similar to that of forsterite and needs no further comment, except to state that, due to the breaking of translational symmetry, several improper symmetry modes occur in the low-wavenumber region containing the external vibrations. Figures 6, 7, and 8 describe the temperature behavior of three different totally symmetric A_g modes for both olivines. Mode wavenumbers and the full widths at half height (FWHH) were recorded in a series of heating and cooling measurements. The three modes can be assigned to different vibration types that have a certain atomic or polyhedral character, and in order to study the effect of temperature on the olivine structure,

Table 2 Symmetry and wavenumbers for the Raman modes of forsterite and their isotope shift, $\Delta\omega$, for $^{26}Mg_2SiO_4$. Possible first-order mode assignments are also listed

Symmetry	ω (cm^{-1})	$\Delta\omega$ (cm^{-1})	ω (%)	Assignment		
				Chopelas (1991)	Rao et al. (1988)[b]	This work
A_g	184.2	2.5	1.34	$T(SiO_4)$	$T(SiO_4)$ + M2	$T(SiO_4)$ + M2
A_g	227.2	1.6	0.70	$T(SiO_4)$	$T(SiO_4)$	”
B_{2g}	243.2	1.8	0.74	mix $R(SiO_4)$	R,$T(SiO_4)$ + M2	”
A_g	303.9	4.2	1.38	M2	R,$T(SiO_4)$ + M2	$R(SiO_4)$ + M2
$B_{1g} + B_{3g}$	316[a]	2.2	0.70	$R(SiO_4) - (B_{1g})$ + mix$R(SiO_4) - (B_{3g})$	R,$T(SiO_4)$ + M2	”
A_g	329	4.6	1.40	$R(SiO_4)$	$R(SiO_4)$ + M2	”
A_g	339	3.4	1.00	M2	M2	”
B_{3g}	373.2	3.5	0.94	mix M2	$R(SiO_4)$ + M2	”
B_{3g}	409	0.0	0.00	v_2		v_2
A_g	421	1.1	0.26	v_2		v_2
$B_{1g} + B_{2g}$	433.6[a]	2.0	0.46	$v_2(B_{1g}) + v_2(B_{2g})$		$v_2(B_{1g}) + v_2(B_{2g})$
A_g	544	0.2	0.04	v_4		v_4
$B_{1g} + B_{2g} + B_{3g}$	588[a]	1.3	0.22	$v_4(B_{1g}) + v_4(B_{2g})$ + $v_4(B_{3g})$		$v_4(B_{1g}) + v_4(B_{2g})$ + $v_4(B_{3g}$
A_g	608	0.0	0.00	v_4		v_4
A_g	824	0.1	0.01	$v_1 + v_3$		$v_1 + v_3$
B_{1g}	838	0.8	0.10	$v_1(+v_3)$		$v_1(+v_3)$
A_g	856	0.3	0.04	$v_1 + v_3$		$v_1 + v_3$
B_{1g}	866	0.9	0.10	$v_3(+v_1)$		$v_3(+v_1)$
B_{2g}	882	0.3	0.03	v_3		v_3
B_{3g}	920	0.4	0.04	v_3		v_3
A_g	966	0.1	0.01	v_3		v_3

[a] Overlapped bands, $T(SiO_4) \Rightarrow$ translation, $R(SiO_4) \Rightarrow$ libration, M2 $\Rightarrow$ translation
[b] Main components of the eigenvectors are considered

they were examined and analyzed in detail. They are the low-wavenumber lattice modes at ~220 and ~300 cm^{-1} and the internal SiO_4 stretching mode at ~850 cm^{-1}. In forsterite all three modes decrease in wavenumber with increasing temperature with no overt breaks or discontinuities (Figs. 6a, 7a, and 8a). There are slight differences in the measured mode wavenumbers at the different temperatures between the heating and cooling experiments in some cases, which may be due, in part, to hysteresis effects. However, we note that the measured wavenumber for all three modes at the lowest temperature is identical prior to heating and after cooling. The spectra of the $Fo_{90}Fa_{10}$ crystal, unlike the spectra of forsterite, show a small discontinuity in the wavenumber behavior for the mode at ~220 cm^{-1} at 700–1000 °C upon heating and cooling. The other two modes at ~300 and ~850 cm^{-1} show no obvious discontinuities or breaks in their wavenumber behavior. All three modes in $Fo_{90}Fa_{10}$ exhibit measurable hysteresis effects in the wavenumber and FWHH behavior (Figs. 6, 7, and 8). Mode wavenumbers are slightly greater and the FWHHs are slightly less upon cooling.

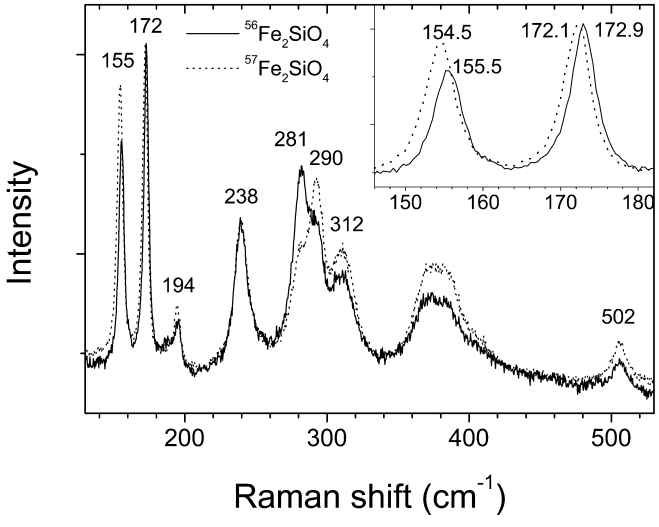

Fig. 3 Raman powder spectra of normal and isotopically enriched fayalite in the low-wavenumber region

Discussion

Crystal chemistry, lattice dynamics, and Fe–Mg partitioning behavior in olivine

A polyhedral model of the olivine structure is presented in Fig. 1 and it shows the salient features. The SiO_4 groups are isolated from one another and have strong internal bonding, but are fixed in a crystal field and thus distorted from ideal T_d to C_s symmetry. This distortion gives rise to different numbers of vibrations compared to the case with ideal tetrahedral symmetry. The structure contains chains of edge-sharing octahedral that run parallel to [001]. The M(1) octahedra share 6 of their 12 edges with other polyhedra. The M(2) octahedra have only three shared edges. M(1) is

Table 3 Symmetry and wavenumbers of the observed Raman modes in normal fayalite and their isotope shift, $\Delta\omega$, in $^{57}Fe_2SiO_4$

Symmetry	ω (cm^{-1})	$\Delta\omega$ (cm^{-1})	$\Delta\omega$ (%)	Assignment	
				Chopelas (1991)	This work
B_{1g}	155.5	1.0	0.7	$T(SiO_4)$[a]	$T(SiO_4)$ + M(2)
A_g	172.9	0.8	0.5	$T(SiO_4)$	,,
B_{1g}	194	0.4	0.2	$T(SiO_4)$	,,
A_g	238	0.0	0.0	M(2)	$T(SiO_4)$
B_{3g}	281	1.0	0.4	Mix M2	$R(SiO_4)$ + M2
A_g + B_{2g}	290	0.3	0.1	$R(SiO_4)$[b] mix M2	$R(SiO_4)$
B_{1g}	312	0.0	0.0	M2[c]	,,
A_g	367	0.0	0.0	v_2	v_2
B_{1g}	384	0.0	0.0	v_2	v_2
B_{2g}	404	0.0	0.0	v_2	v_2
A_g	502	0.0	0.0	v_4	v_4

[a] $T(SiO_4) \Rightarrow$ translation
[b] $R(SiO_4) \Rightarrow$ libration
[c] M2 $\Rightarrow$ translation

slightly smaller than M(2) and is more irregular in geometry. Divalent Mg and Fe occur at M(1) and M(2), where the bonding is weaker than in a SiO_4 tetrahedron (e.g., the Pauling bond strength is proportional to Z/n, where Z and n are the cation valence and coordination number, respectively). Thus, their vibrations occur at relatively low energies and are strongly a function of the crystal-chemical environment in which they occur. Rao et al. (1988) show nicely, using inelastic neutron-scattering results and lattice-dynamic calculations, the partial phonon density of states for Mg and SiO_4 (external and internal) vibrations in forsterite. The internal SiO_4 vibrations occur in two "envelopes" between 1200 and 800 cm^{-1}, the external vibration of the SiO_4 groups occur at wavenumbers mostly below 400 cm^{-1}, and the octahedrally coordinated Mg cations have vibrations between 0 and 600 cm^{-1}. Thus, the division between internal and external vibrations has validity.

Indeed, published Raman and IR spectra of olivine show a separation between high-wavenumber internal SiO_4 vibrations and lower-wavenumber lattice vibrations consisting of M cation and external SiO_4 vibrations (Hohler and Funk 1973; Stidham et al. 1976; Hofmeister 1987; Rao et al. 1988; Chopelas 1991). For vibrational spectra only M(2) translations are Raman-active, while in the IR both M(1) and M(2) vibrations are present. Assignments for the internal SiO_4 vibrations are now understood and agreed upon and we adopt those of Chopelas (1991; see Tables 2 and 3). Mode assignments for the external vibrations associated with the SiO_4 groups and the M(2) vibrations pose a more difficult problem, because most are mixed and coupled vibrations (see, for example, Rao et al. 1988 for an analysis of the eigenvectors and eigenvalues for the atoms in forsterite). Many have a large specific vibrational character, however, that can be experimentally determined.

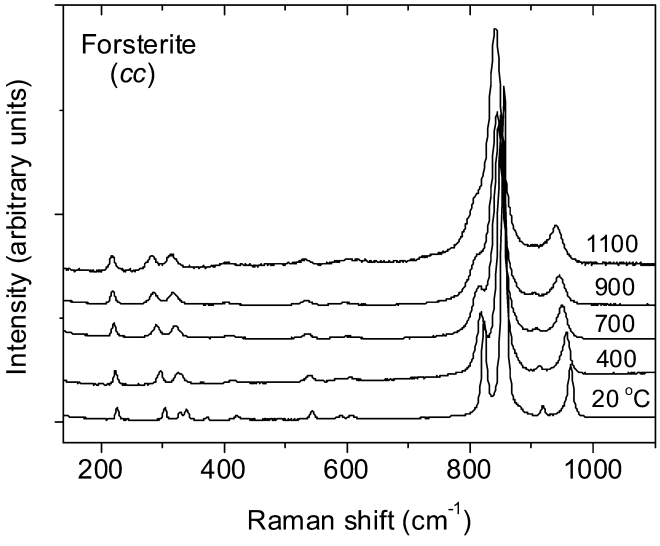

Fig. 4 Polarized (*cc*) single-crystal Raman spectra of forsterite between room temperature and 1200 °C

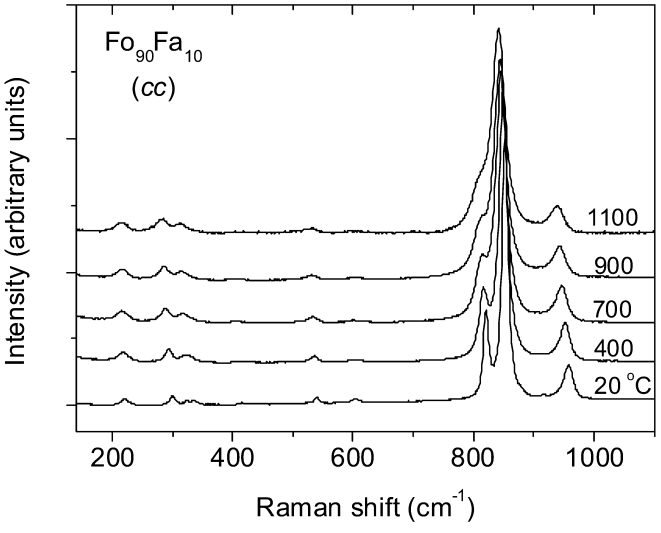

Fig. 5 Polarized (*cc*) single-crystal Raman spectra of $Fo_{90}Fa_{10}$ between room temperature and 1200 °C

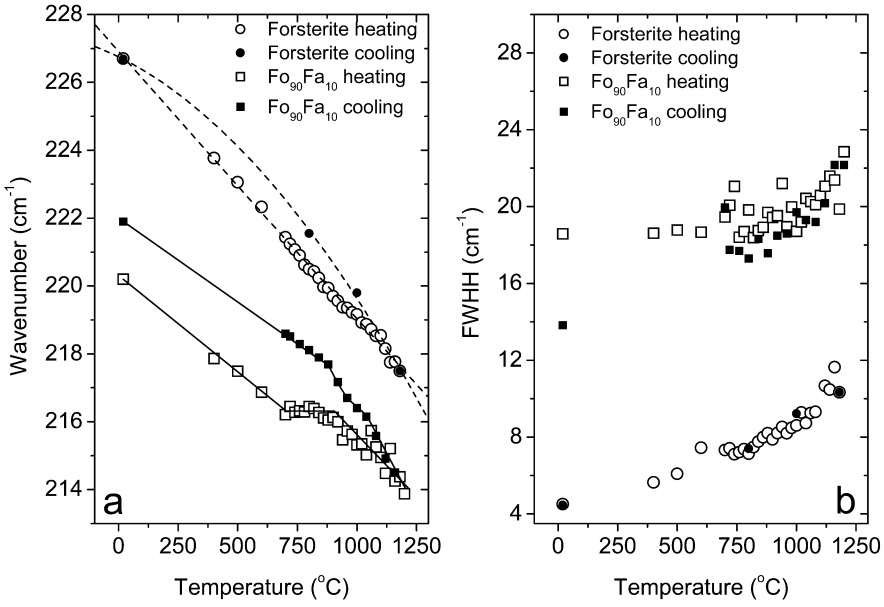

Fig. 6 **a** Temperature dependence of the wavenumber and **b** FWHH of the A_g mode at 220 cm^{-1} in Fo_{100} and $Fo_{90}Fa_{10}$

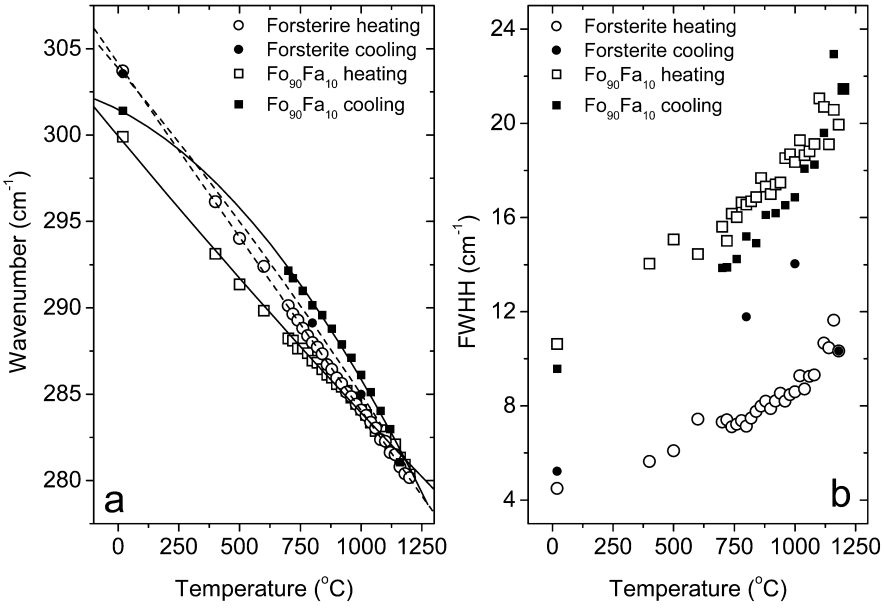

Fig. 7 **a** Temperature dependence of the wavenumber and **b** FWHH of the mode at 300 cm^{-1} in Fo_{100} and $Fo_{90}Fa_{10}$

A number of room-temperature X-ray diffraction and ^{57}Fe Mössbauer investigations have been made to determine the structural state (i.e., partitioning behavior) in Mg–Fe olivine solid solutions (see review by Brown 1980; and later works of Princivalle and Secco 1985; Kirfel 1996). From the different studies, it is concluded that Fe^{2+} and Mg are approximately disordered over M(1) and M(2) or that Fe^{2+} shows a slight preference for the smaller M(1) site. However, in forsterite-rich (Fo_{80} to Fo_{92}) compositions Mg may show a very slight preference for M(1) (Princivalle and Secco 1985). This view of the ordering behavior in olivine underwent a major change following recent in-situ high-temperature neutron diffraction investigations. Artioli et al. (1995) determined the partitioning behavior of Fe^{2+} and Mg in a natural single-crystal olivine of composition $Fo_{88}Fa_{12}$ between 25 and 1060 °C. The behavior can be described by the cation partition coefficient (K_D) for the intracrystalline exchange reaction $Fe_{M(2)} + Fe_{M(1)} = Fe_{M(1)} + Fe_{M(2)}$. It is defined as:

$$K_D = [Fe_{M(1)} \cdot Mg_{M(2)} / Fe_{M(2)} \cdot Mg_{M(1)}] \ . \quad (1)$$

At room temperature to about 880 °C $K_D \geq 1$, but above 900 °C there is a reversal in the ordering behavior and $K_D < 0.7$ (Artioli et al. 1995). Rinaldi et al. (2000)

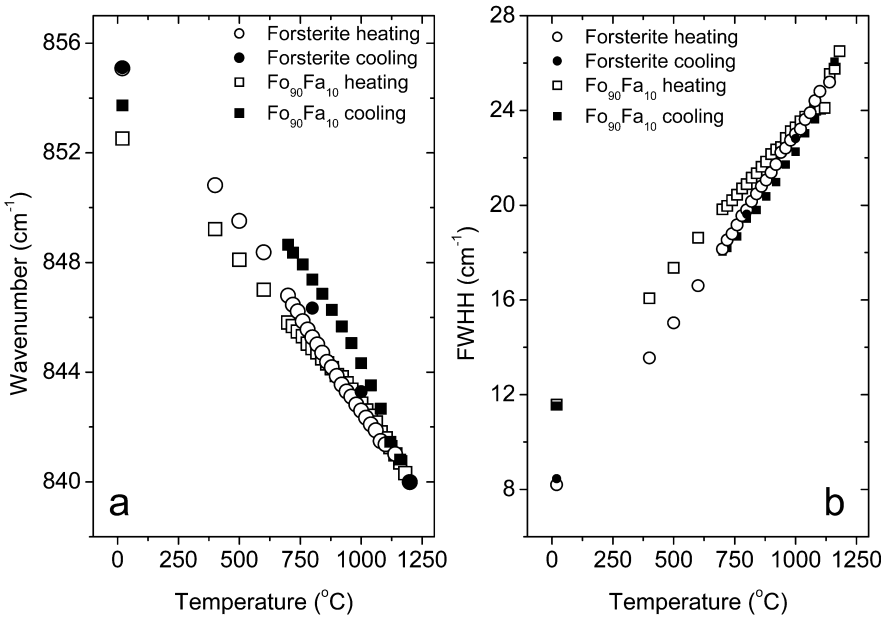

Fig. 8 **a** Temperature dependence of the wavenumber and **b** FWHH of the mode at 850 cm^{-1} in Fo_{100} and $Fo_{90}Fa_{10}$

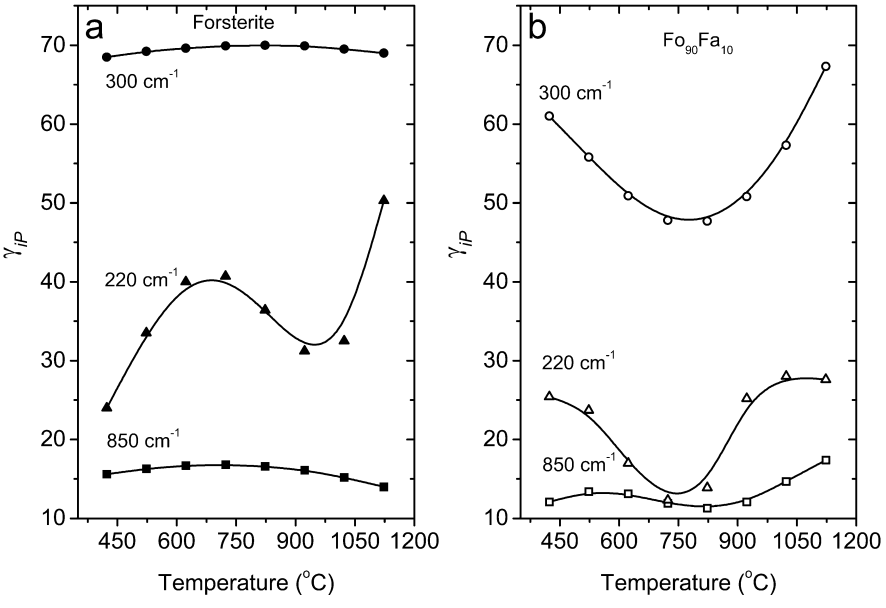

Fig. 9 **a** Temperature dependence of the isobaric mode Grüneisen parameter for three different A_g modes in forsterite and **b** $Fo_{90}Fa_{10}$

made further neutron diffraction measurements on two olivine single crystals of composition $Fo_{88}Fa_{12}$ and $Fo_{90}Fa_{10}$ and showed that above 900 °C Fe^{2+} progressively partitions into the M(2) site and $K_D \approx 0.2$ at 1300 °C. Redfern et al. (2000) deduced similar ordering behavior from powder neutron diffraction measurements made on a more fayalite-rich synthetic $Fa_{50}Fo_{50}$ sample. The variations in ordering state were attributed by Artioli et al. (1995) to a change in the vibrational properties of the cations on the M(1) and M(2) sites. They proposed that an increase in vibrational entropy, as described by the diffraction-determined atomic displacement parameters, could counter the decrease in configurational entropy accompanying increased ordering, and could be the main driving force for greater cation ordering at high temperature.

Mode assignments based on $^{26}Mg \Rightarrow {}^{24}Mg$ and $^{57}Fe \Rightarrow {}^{56}Fe$ isotope substitution

Forsterite

It is evident from the data in Table 2 that the Raman spectrum of forsterite can be divided into two wavenumber regions. External SiO_4 and Mg vibrations are

located between 150 and 400 cm^{-1} and internal SiO_4 vibrations between 400 and 1000 cm^{-1}. This follows from the observed isotopic-related mode shifts related to $^{26}Mg \Rightarrow {}^{24}Mg$ substitution. The high-wavenumber region can, in turn, be divided into subregions of v_2 (400–500 cm^{-1}) and v_4 bending (500–610 cm^{-1}) and coupled v_1–v_3 stretching vibrations (800–1000 cm^{-1}). Based on the observed isotopic mode shifts (Table 2), it must be concluded that there are no pure Mg translations. For a pure Mg translation, the isotopic shift would be given approximately by $(26/24.3)^{1/2} \Rightarrow 3.4\%$, while the largest observed shift is 1.4%. The low-wavenumber vibrations are therefore mixed modes consisting of Mg-cation translations and $R(SiO_4)$ and $T(SiO_4)$ vibrations. The A_g modes at ~184, 304, and 329 cm^{-1} have the largest Mg character. In other orthosilicates such as garnet it has been shown (Kolesov and Geiger 1998) that the $R(SiO_4)$ vibrations (i.e., librations) generally lie between 300 and 400 cm^{-1}, and the translations of SiO_4 groups, $T(SiO_4)$, are usually about one half to two thirds less in energy, that is roughly around 200 cm^{-1}. Our first-order description of the low-wavenumber region gives Mg–$T(SiO_4)$ mixed modes between 170 and 250 cm^{-1} and Mg–$R(SiO_4)$ mixed modes between 300 and 400 cm^{-1}. Chopelas (1991) assigned the totally symmetric Raman modes at 304 and 339 cm^{-1} to Mg-cation translations. Indeed, both of these modes exhibit measurable isotopic shifts of 1.4 and 1.0%, respectively, but they are better described as mixed modes (see also Rao et al. 1988). A more quantitative higher-order description of these modes, however, would give more complex mixed modes involving $T(SiO_4)$, Mg and $R(SiO_4)$ vibrations (Rao et al. 1988). In order to make such an analysis further lattice-dynamic calculations are required, which incorporate the isotopic shifts measured in this work, to define more quantitatively the eigenvalues and eigenvectors for the different atoms.

Fayalite

The high-wavenumber region in the spectrum of fayalite shows noticeable differences compared to that in forsterite and tephroite in terms of the line widths of the modes (Kolesov and Geiger, accompanying manuscript). The SiO_4 mode at 814 cm^{-1} is about 1.5 larger and the mode at 840 cm^{-1} about 3.5 larger than the equivalent modes in forsterite and tephroite. In the low-wavenumber region strong differences, compared to the spectrum of forsterite, arise from the presence of the heavier Fe^{2+} cation. Four bands at ~155 cm^{-1} (B_{1g}), 172 cm^{-1} (A_g), 194 cm^{-1} (B_{1g}), and 281 cm^{-1} (B_{3g}) display measurable shifts related to the isotope effect (Fig. 3). As in the case for Mg in forsterite, the largest measured isotopic shifts (0.7%) are less than the maximum possible value for a pure Fe vibration [$^{57}Fe \Rightarrow {}^{56}Fe : (57/55.8)^{1/2} \Rightarrow 1.0\%$. The largest isotopic shifts are observed for the modes at 155 and 171 cm^{-1} and the mode at 281 cm^{-1} located in the general wavenumber region of the $R(SiO_4)$ modes. The B_{1g} mode at 155 cm^{-1} has a strong Fe character. The $T(SiO_4)$ mode at 238 cm^{-1} and the $R(SiO_4)$ modes at 290 and 312 cm^{-1} are also relatively pure. Our first-order mode assignments are given in Table 3.

Mode behavior as a function of temperature and Fe–Mg order–disorder

Forsterite and $Fo_{90}Fa_{10}$

In order to understand the effect of temperature on the olivine structure, the microscopic isobaric Grüneisen parameter for the three symmetric A_g modes at ~220, ~300, and ~850 cm^{-1} at room temperature were calculated and analyzed. The relationship used is (Mammone and Sharma 1979; Gillet et al. 1989):

$$\gamma_{iP} = (-1/\alpha)(\partial \ln v_i/\partial T)_P \ , \qquad (2)$$

where v_i is the wavenumber of the ith mode and α is the bulk thermal expansion. The temperature-dependent thermal expansion coefficient for forsterite was used to calculate γ_{iP} for both olivine compositions and is that taken from Anderson and Suzuki (1983). According to them, α changes nonlinearly between 0 and 300 °C and is a monotonic and nearly linear function of temperature between 400 and 1200 °C. Figure 9 shows the calculated γ_{iP} values for forsterite and $Fo_{90}Fa_{10}$ as a function of temperature.

For forsterite the Grüneisen parameters for the modes at about 300 and 850 cm^{-1} are nearly temperature-independent, while that for the mode at about 220 cm^{-1} is not. The values of γ_{iP} for the mode at 850 cm^{-1} are small, because the Si–O bond is strong (see also Gillet et al. 1991), while the large values for the 300-cm^{-1} mode can be explained by the weaker Mg–O bond. The mode at 220 cm^{-1}, which is a mixed Mg/$T(SiO_4)$ vibration, has an intermediate value and it varies with temperature in an unusual manner. We think that its behavior could reflect small structural changes possibly resulting from rotation of the rigid SiO_4 tetrahedra with changing temperature. We think this, because the energy of $T(SiO_4)$ vibrations should be largely a function of the intertetrahedral Mg–O and O–O interactions. However, the total O–O interaction does not vary significantly with temperature (see below), and we conclude that a rotation of the SiO_4 groups can best explain the observed temperature dependence. In other words, the "intermolecular" interactions vary more as a function of temperature than the internal force constants of the SiO_4 groups. The actual situation is, of course, more complicated, and our conclusions should be considered hypothetical. This is because the analysis does not consider any effects related to anisotropic thermal expansion and because the bulk thermal expansion was used in the calculations. It would also be more correct to consider explicitly the thermal expansions of the different M(1) and M(2) and SiO_4 polyhedra for the calculation

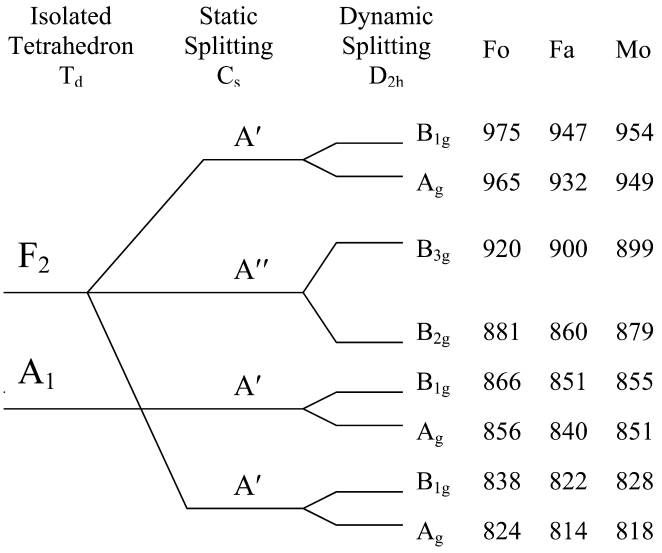

Fig. 10 Schematic representation of the crystal (static) and correlation (dynamic) splitting of the v_1 and v_3 modes of the SiO_4 tetrahedron in olivine structures and their wavenumbers in cm^{-1}. *Fo* forsterite; *Fa* fayalite; *Mo* monticellite. *A′* and *A″* denote the symmetry types for the C_s site symmetry

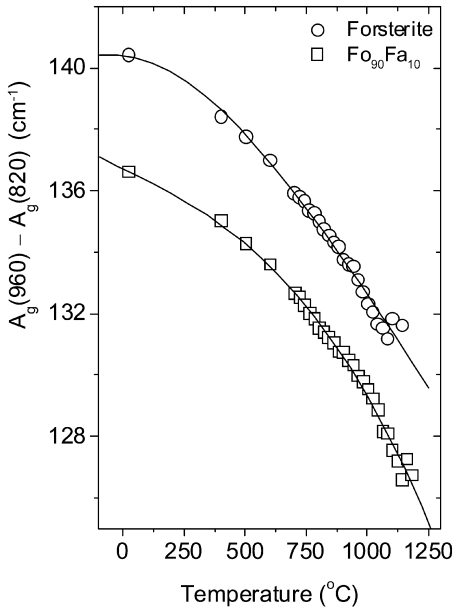

Fig. 11 Wavenumber difference between the crystal field split coupled $v_1 - v_3$ stretching modes in forsterite and $Fo_{90}Fa_{10}$ as a function of temperature

of the Grüneisen parameters for the different mode types.

For $Fo_{90}Fa_{10}$, the first-order behavior (i.e., the relative values) of the different γ_{iP} mode parameters is similar to that in forsterite. There are, however, notable differences. For example, the values for the Grüneisen parameters for the modes at about 220 and 300 cm^{-1} first decrease and then increase between 450 and 1150 °C. The decrease in γ_{iP} from 400 to 750 °C and then an increase from 750 to 1100 °C may arise from: (1) a different temperature-dependent structural behavior for $Fo_{90}Fa_{10}$ versus that for forsterite or (2) the presence of measurable concentrations of lattice defects and/or structural heterogeneity related to the distribution of Fe and Mg in the natural $Fo_{90}Fa_{10}$ crystal. In order to address both of these possibilities, we consider the wavenumber behavior of these two modes (Figs. 6 and 7). As for possibility (1), rotation of the SiO_4 tetrahedra with changes in temperature will produce structural distortions, and upon cooling the time associated with distortional damping could possibly give rise to mode-energy hysteresis at intermediate temperatures. The melting point of forsterite is ~1900 °C and it is much greater than the maximum temperature of the measurements (i.e., ~1200 °C). The melting point of fayalite is, in comparison, much lower ~1200 °C, and its structural distortions at a given temperature should be larger compared to those in forsterite. The $Fo_{90}Fa_{10}$ crystal has a lower melting temperature and thus its corresponding structural distortions should also be greater than in forsterite. This can possibly account for the larger hysteresis effects for the mode behavior in the spectra of $Fo_{90}Fa_{10}$ versus that in the spectra of forsterite. As for possibility (2), Figs. 6b and 7b, and to a lesser extent Fig. 8b, show that the FWHH of the three A_g bands for $Fo_{90}Fa_{10}$ are greater than those for forsterite. This broadening is related to structural heterogeneity in the solid-solution crystal that is a function of the local Fe–Mg distribution. End-member forsterite has no composition-related local structural heterogeneity. However, it should be noted that the band at about 220 cm^{-1} and also the band at 850 cm^{-1} for $Fo_{90}Fa_{10}$ become slightly

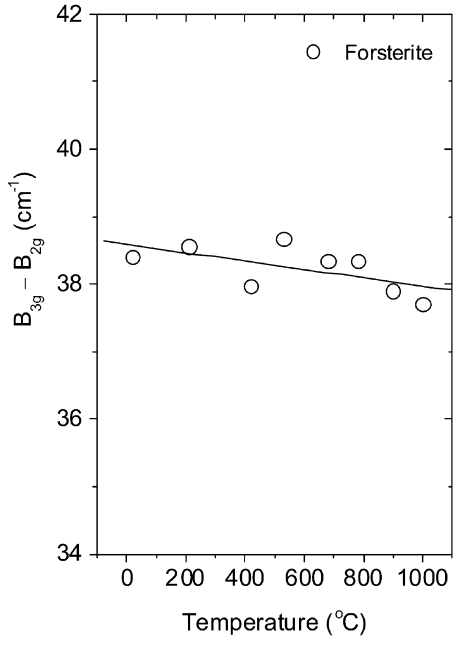

Fig. 12 Wavenumber difference between the dynamically split B_{3g} mode and the B_{2g} mode in forsterite

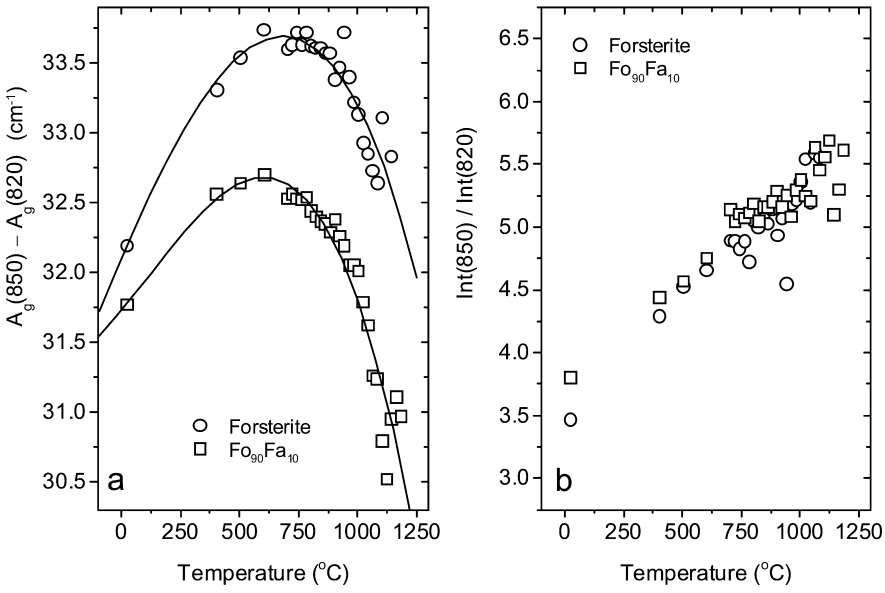

Fig. 13 **a** Wavenumber difference between the coupled v_1–v_3 modes of A_g symmetry and **b** the ratio of their intensities in forsterite and $Fo_{90}Fa_{10}$ as a function of temperature

narrower upon cooling, although the degree of intracrystalline Fe–Mg disorder should become greater with decreasing temperature (Artioli et al. 1995; Rinaldi et al. 2000). Band broadening is usually associated with increased cation disorder. In addition to Fe–Mg order–disorder effects, various types of lattice defects (Schottky or Frenkel type, etc.) may also play a role in affecting the bandwidths. One can propose for the modes in $Fo_{90}Fa_{10}$ that the observed FWHH behavior is reflecting not just structural variations related to the cation distribution state, but also the annealing out of lattice defects at high temperature.

We consider the nature of structural variations in olivine as a function of temperature in greater detail. The wavenumber behavior of the mode at $\sim$220 cm^{-1} is shown in Fig. 6 for both crystals. It is the only mode that shows small discontinuities in its wavenumber behavior as a function of temperature and only for $Fo_{90}Fa_{10}$. The discontinuities occur between 700 and 1000 °C and they are observed in both the heating and cooling measurements. The analogous mode in forsterite, whose structure cannot have any cation order–disorder, shows no experimentally significant discontinuities. Two possible physical effects could account for the behavior of this mode in $Fo_{90}Fa_{10}$: (1) abrupt structural modifications (e.g., rigid SiO_4 tetrahedral rotation) could cause the discontinuities in the wavenumber behavior or (2) Mg and Fe^{2+} may begin to significantly redistribute over the M(1) and M(2) sites in this temperature range. As to (1), the intertetrahedral oxygen–oxygen force constants do not change significantly over this temperature interval (as discussed in the next section) and thus sudden structural variations probably cannot account for the observed wavenumber behavior. As for (2), the mode at $\sim$220 cm^{-1} has a mixed $T(SiO_4)$/M(2) character with a measurable M(2)-site component. It could, therefore, reflect changes in the intracrystalline Mg–Fe^{2+} partitioning behavior. An increase in mass at the M(2) site should cause a decrease in wavenumber of a $T(SiO_4)$/M(2) vibration, or alternatively a decrease in mass at M(2) should cause an increase in wavenumber. The mode at $\sim$220 cm^{-1} in the spectra of the $Fo_{90}Fa_{10}$ crystal shows a linear decrease in wavenumber with increasing temperature upon which slight discontinuities are superimposed beginning at about 700 °C. Thus, the discontinuity could possibly be related to a small decrease in the concentration of Fe^{2+} at M(2). On the other hand, from the measurements made on cooling, the intracrystalline cation partitioning state is difficult to interpret from the wavenumber behavior. The state of reordering in olivine is very fast at temperatures above 800–900 °C and should, in principle, be observable in the mode behavior upon heating and cooling at the highest temperatures.

The wavenumber behavior of the two modes at about 300 and 850 cm^{-1} can also be used to investigate the intracrystalline partitioning state (Figs. 7 and 8). Both modes show smooth variations in their wavenumber behavior as a function of temperature in both heating and cooling experiments. No overt anomalies or discontinuities as a function of temperature can be observed. The mode at 300 cm^{-1}, especially, has measurable M(2) character, but it shows no features that would indicate a change in the partitioning state of Mg and Fe at M(2).

We conclude that the partitioning behavior in the $Fo_{90}Fa_{10}$ crystal is difficult to determine quantitatively from our Raman spectra, and also to link to the neutron diffraction results made at high temperatures. These first Raman results cannot exclude the possibility of some change in the ordering state, because small discontinuities in the wavenumber behavior of the mode at $\sim$220 cm^{-1} appear to be present. Further in-situ single-crystal Raman measurements are required on more iron-

rich olivine crystals in order to address more fully the partitioning behavior of Fe^{2+} and Mg. In the case of more iron-rich crystals, it can be expected that the modes would show larger wavenumber variations or discontinuities than for Fe-poor crystals, if significant changes in the partitioning behavior of Mg and Fe^{2+} do indeed occur.

Internal SiO_4 modes – static crystal- and dynamic-field splitting and coupling

Four internal vibrations of different symmetry and energy would characterize an undistorted SiO_4 tetrahedron of T_d symmetry. These are the asymmetric $v_3(3)$ and symmetric v_1 stretching vibrations and the $v_4(3)$ and $v_1(2)$ bending vibrations, where the numbers in parenthesis indicate the degeneracy. When a tetrahedron is distorted as a result of static crystal-field forces, for example, the degeneracy can be lifted and additional modes can arise. Mode splitting can also result from dynamical interactions between the isolated SiO_4 groups. In addition to this mode splitting, coupling between the different modes can also occur and all of these effects lead to a complicated lattice-dynamic behavior in olivine, as shown by Hohler and Funk (1973). There has been considerable work done to study and explain the phenomena. For example, in monticellite it was observed that the v_1-derived mode at 852 cm^{-1} has a greater wavenumber than the v_3-derived mode at 817 cm^{-1}, although this behavior is contrary to the normal case for the energies of internal vibrations of an undistorted tetrahedron (Piriou and McMillan 1983). These workers investigated the nature of mode splitting and coupling of internal SiO_4 modes for different end-member composition olivines and related structures using their Raman spectra and their known crystal-chemical properties, and they were able to explain the observed "reversal" in the v_1–v_3 mode energies. We analyze the effect of temperature on v_1–v_3 coupling because this has not been done before.

First, however, we consider briefly SiO_4 mode splitting. Figure 10 shows schematically both the static-crystal and dynamic-field splitting for internal SiO_4-stretching vibrations of different end-member olivines (i.e., Fo, Fa, and Mo) as determined from their Raman spectra. The F_2 symmetry v_3 stretching vibration of an undistorted tetrahedron splits in the olivine crystal field into six different modes. For forsterite they are located at 824, 838, 882, 920, 966, and 975 cm^{-1}, for example. The temperature dependence of the wavenumber for the two A_g modes at ~965 and ~824 cm^{-1} in both forsterite and $Fo_{90}Fa_{10}$ are considered in order to better understand how the various intra and interpolyhedral interactions give rise to this splitting. These two modes are the highest and lowest symmetric energy states of a split v_3 vibration, and they reflect the strength of the crystal-field splitting resulting from thermally induced structural expansion or contraction. The difference in wavenumber between the two modes (Fig. 11) in both olivine crystals decreases slightly with increasing temperature reflecting, as expected, a small weakening of the crystal-field splitting. The degree of dynamical splitting, in comparison, is given by the temperature-dependent wavenumber difference between any two vibrations that are dynamically split, for example, the B_{3g} (920 cm^{-1}) mode and the B_{2g} (882 cm^{-1}) mode in forsterite (Fig. 10). Figure 12 shows their corresponding wavenumber difference as function of temperature. The change is very slight, if existent at all, and thus dynamic splitting, unlike static crystal-field splitting of the internal SiO_4 vibrations, is largely independent of temperature. Because it is largely controlled by intertetrahedral O–O interactions, it can be concluded that thermally induced expansion of the forsterite structure does not lead to a major weakening of the interactions between SiO_4 groups. Moreover, because the degree of dynamic splitting remains constant as a function of temperature, rigid SiO_4 tetrahedral rotation does not affect the total O–O intertetrahedral interactions. As discussed earlier, SiO_4 rotation is thought to control to a large extent the energy of $T(SiO_4)$ vibrations. Therefore, the mixed $T(SiO_4)$/M(2) mode at ~220 cm^{-1} is not affected by SiO_4 rotation occurring as a function of temperature.

The symmetric SiO_4 stretching vibration at ~820 cm^{-1} (note: this mode is asymmetric for a free SiO_4 tetrahedron of T_d symmetry, but it is symmetrical in the olivine structure. That is, this mode is a symmetric stretching vibration derived from an asymmetrical v_3 mode) and the symmetric stretching mode at ~856 cm^{-1} are coupled to one another. The change in the strength of their coupling in both forsterite and $Fo_{90}Fa_{10}$, as described by their wavenumber difference as a function of temperature, is depicted in Fig. 13a. The change in the difference is very small and thus the degree of coupling is temperature independent. However, this behavior may not accurately reflect the true coupling behavior, because the energy of the ~820-cm^{-1} mode is also a function of two other factors, namely: (1) the degree of the static crystal-field splitting (Fig. 11), and (2) the shift in the "center of gravity" of the energy of the v_1 and v_3 modes. Thus, a rigorous analysis of the degree of v_1–v_3 coupling is not possible as based solely on their temperature-dependent wavenumber behavior. More can be determined, if one considers the ratioed intensities of the two modes as a function of temperature (Fig. 13b). In this case, the band at ~850 cm^{-1} increases in intensity relative to the band at ~820 cm^{-1} with increasing temperature. For a tetrahedron of T_d symmetry, the Raman intensity of the asymmetric v_3 mode is usually less than the intensity of the symmetric v_1 mode. However, in a distorted tetrahedron a split component of the v_3 mode, which is coupled to v_1, can increase in intensity because of the coupling. Therefore, the relative decrease in intensity of the mode at ~820 cm^{-1} with increasing temperature means that it has a stronger v_3 character than the mode at ~850 cm^{-1} and also that the coupling becomes weaker at higher temperatures.

Acknowledgements We thank Prof. H. Rager (Marburg) and Dr. F. Wallrafen (Bonn) for the donation of olivine single crystals. This research was made possible by grant I/72 951 from the VolkswagenStiftung. The comments of two reviewers led to changes that improved the manuscript.

References

Anderson OL (1996) Anharmonicity of forsterite and the thermal pressure of insulators. Geophys Res Lett 23: 3031–3034

Anderson OL, Suzuki I (1983) Anharmonicity of three minerals at high temperature: forsterite, fayalite and periclase. J Geophys Res 88: 3549–3556

Artioli G, Rinaldi R, Wilson CC, Zanazzi PF (1995) High-temperature Fe–Mg cation partitioning in olivine: in-situ single-crystal neutron-diffraction study. Am Min 80: 197–200

Bershov LV, Gaite J-M, Hafner SS, Rager H (1983) Electron paramagnetic resonance and ENDOR studies of Cr^{3+}-Al^{3+} pairs in forsterite. Phys Chem Miner 9: 95–101

Brown, GE, J (1980) Olivines and silicate spinels. In: Ribbe PH (ed) Orthosilicates, Reviews in Mineralogy, vol 5. Mineralogical Society of America, Washington, DC, pp 275–381

Chopelas A (1990) Thermal properties of forsterite at mantle pressures derived from vibrational spectroscopy. Phys Chem Miner 17:149–156

Chopelas A (1991) Single crystal Raman spectra of forsterite, fayalite, and monticellite. Am Mineral 76: 1101–1109

Ghose S, Hastings JM, Choudhury N, Chaplot SL, Rao KR (1991) Phonon dispersion relation in fayalite, Fe_2SiO_4. Physica (B) 174: 83–86

Gillet P, Guyot F, and Malezieux J (1989) High-pressure and high-temperature Raman spectroscopy of Ca_2GeO_4: some insights on anharmonicity. Phys Earth Planet Inter. 58: 141–154

Gillet P, Richet P, Guyot F, Fiquet G (1991) High-temperature thermodynamic properties of forsterite. J Geophys Res 96: 11805–11816

Gillet P, Daniel I, Guyot F (1997) Anharmonic properties of Mg_2SiO_4-forsterite measured from the volume dependence of the Raman spectrum. Eur J Mineral 9: 255–262

Hofmeister AM (1987) Single-crystal absorption and reflection spectroscopy of forsterite and fayalite. Phys Chem Miner 14: 499–513

Hofmeister AM (1997) Infrared reflectance spectra of fayalite, and absorption data from assorted olivines, including pressure and isotope effects. Phys Chem Miner 24: 535–546

Hohler V, Funk E (1973) Vibrational spectra of crystals with olivine structure. I. Silicates. Z. Naturforsch (B) 28: 125–139

Iishi K (1978) Lattice dynamics of forsterite. Am Miner 63: 1198–1208

Kieffer SW (1985) Heat capacity and entropy: systematic relations to lattice entropy. In: Kieffer SW, Navrotsky A (eds) Microscopic to macroscopic – atomic environments to mineral thermodynamics, Reviews in Mineralogy, vol 4, Mineralogical Society America, Washington, DC, 65–126

Kirfel A (1996) Cation distributions in olivines and orthopyroxenes. An interlaboratory study. Phys Chem Miner 23: 503–519

Kolesov BA, Geiger CA (1998) Raman spectra of silicate garnets. Phys Chem Miner 25: 142–151

Mammone JF, Sharma SK (1979) Pressure and temperature dependence of the Raman spectra of rutile-structure oxides. Carnegie Inst Washington Year Book 78: 369–373

Liu L-G, Mernagh TP (1993) Raman spectra of forsterite and fayalite at high pressures and room temperature. High Press Res 11: 241–256

Pâques–Ledent M Th, Tarte P (1973) Vibrational studies of olivine-type compounds I. The IR and Raman spectra of the isotopic species of Mg_2SiO_4. Spectrochim Acta 29(A): 1007–1016

Piriou B, McMillan P (1983) The high-frequency vibrational spectra of vitreous and crystalline orthosilicates. Am Mineral 68: 426–443

Price DL, Ghose S, Choudhury N, Chaplot SL, Rao KR (1991) Phonon density of states in fayalite, Fe_2SiO_4. Physica (B) 174: 87–90

Princivalle F, Secco L (1985) Crystal structure refinement of 13 olivines in the forsterite–fayalite series from volcanic rocks and ultramafic nodules. Tschermaks Min Pet Mitt 34: 105–115

Rao KR, Chaplot SL, Choudhury N, Ghose S, Hastings JM, Corliss LM, Price DL (1988) Lattice dynamics and inelastic neutron scattering from forsterite, Mg_2SiO_4: phonon dispersion relation, density of states and specific heat. Phys Chem Miner 16: 83–97

Redfern SAT, Artioli G, Rinaldi R, Henderson CMB, Knight KS, Wood BJ (2000) Octahedral cation ordering in olivine at high temperature. II: an in situ neutron powder diffraction study on synthetic $MgFeSiO_4$ (Fa50). Phys Chem Miner 27: 630–637

Rinaldi R, Artioli G, Wilson CC, McIntyre G (2000) Octahedral cation ordering in olivine at high temperature. I: in situ neutron single-crystal diffraction studies on natural mantle olivines (Fa12 and Fa10). Phys Chem Miner 27: 623–629

Schmidt W, Brotzeller C, Geick R, Schweiss P, Treutmann W (1992) Magnon-phonon coupling in Fe_2SiO_4. J Magnet Mag Mat 104–107: 1049–1050

Servoin JL, Piriou B (1973) Infrared reflectivity and Raman scattering of Mg_2SiO_4 single crystal. Phys Status Solidi (B) 55: 677–686

Shannon RD, Subramanian MA, Hosoya S, Rossman GR (1991) Dielectric constants of tephroite, fayalite, olivine and the oxide additivity rule. Phys Chem Miner 18: 1–6

Stidham HD, Bates JB, Finch CB (1976) Vibrational spectra of synthetic single crystal tephroite, Mn_2SiO_4. J Phys Chem 80: 1226–124

Tarte P, Preudhomme J (1970) Use of medium-weight isotopes in infrared spectroscopy of inorganic solids: a new method of vibrational assignments. Spectrochim Acta 26(A): 2207–2219